LANGMUIR

Article

Molecular Simulations of Hydration Behavior of Zwitterion Brush Array and Its Antifouling Property in Aqueous Environment

Yuan Xiang, Rong-Guang Xu, and Yongsheng Leng

Langmuir, **Just Accepted Manuscript** • DOI: 10.1021/acs.langmuir.7b03386 • Publication Date (Web): 23 Jan 2018

ACS Publications

Langmuir is published by the American Chemical Society. 1155 Sixteenth Street N.W., Washington, DC 20036

Submitted to Langmuir on September 27, 2017; revised version submitted on November 28, 2017

Molecular Simulations of Hydration Behavior of Zwitterion Brush Array and Its Antifouling Property in Aqueous Environment

Yuan Xiang, Rong-Guang Xu, and Yongsheng Leng*

Department of Mechanical & Aerospace Engineering, The George Washington University, Washington, D.C. 20052, United States

Abstract: We carried out umbrella sampling and molecular dynamics (MD) simulations to investigate molecular interactions between sulfobetaine zwitterions or between sulfobetaine brushes in different media. Simulation results show that it is more energetically favorable for the two sulfobetaine zwitterions or brushes being fully hydrated in aqueous solutions than in vacuum where strong ion pairs are formed. Structural properties of hydrated sulfobetaine brush array and its antifouling behavior against a foulant gel are subsequently studied through steered MD simulations. We find that sulfobetaine brush arrays with different grafting densities have different structures and antifouling mechanisms. At a comparably higher grafting density, the sulfobetaine brush array exhibits a more organized structure which can hold a tightly bound hydration water layer at the interface. Compression of this hydration layer results in a strong repulsive force. However, at a comparably lower grafting density, the brush array exhibits a randomly oriented structure in which the antifouling of the brush array is through the deformation of the sulfobetaine branches.

* Corresponding author, Tel.: 202-994-5964; e-mail: leng@gwu.edu.

1. INTRODUCTION

Membrane separation is a widely used technology in water purification.[1-6] However, the major deficiency of this technique is fouling problem[7-9] induced by the accumulation of foreign substances on the membrane surface. Membrane fouling can significantly reduce the membrane performances, such as water flux and effluent quality. One of the promising techniques to resolve the fouling problem is to modify the surface chemistry of membrane, which can also improve other properties of membrane, such as salt rejection, chlorine tolerance, and thermal stability.[10] Among many antifouling monomers, polyethylene glycol (PEG) and polyzwitterion (PZ) coatings grafted onto membrane surfaces[11-16] are promising candidates of antifouling materials. Although PEG has a good antifouling property due to its ability to bind water molecules (hydration property), it also suffers from oxidization susceptibility and thus may not be a good choice for long-term applications.[17] Compared with PEG coatings, PZ coatings, such as poly(carboxybetaine) (pCB) and poly(sulfobetaine) (pSB), are more chemically stable and could bind water molecules even stronger than PEG via localized charges,[18] making them excellent antifouling materials. A PZ molecule contains both positively and negatively charged functional groups within the same side chain, keeping its total charge neutrality. In recent years, many methods have been proposed to create PZ coatings on polyamide membrane surface, including chemical vapor deposition,[19] click chemistry[20] and concentration-polarization-enhanced radical graft polymerization.[21] PZ coatings exhibit more stable chemical properties than PEG in the presence of oxygen and transition metal ions, and therefore have received growing interests not only in membrane technology, but also in marine, biomedical, and other antifouling applications.[18-31]

Currently, most investigations of PZ coatings focus on grafting methodology or designs of PZ interfaces.[32, 33] However, the detailed structural properties of zwitterionic coating at the interface and its fundamental antifouling mechanism from molecular perspective are still not fully understood.[34-36] For example, what are the hydration structures of zwitterionic brush arrays at the interface and how does a foulant molecule interact with the zwitterionic coating when they are in close proximity? Moreover, how does the grafting density of zwitterionic brushes influence this foulant-coating interaction? These are the fundamental questions that are critical to the molecular design of antifouling materials in membrane technology.

Many theoretical studies through molecular dynamics (MD) simulations have been carried out recently to understand the structural properties of polyamide membranes [37-43] and zwitterionic materials.[44-51] These simulations provide molecular details that are not directly available from experiments. In particular, hydration behaviors of zwitterions and their association with metal ions were reported by Shao *et al*,[45, 46] in which they found that carboxybetaine associated more strongly with Li^+ and Na^+ (smaller ions), while sulfobetaine associated more strongly with K^+ and Cs^+ (larger ions). High ion rejection of zwitterion functionalized carbon nanotubes (CNTs) was reported by Chan et al.[49] They also calculated the upper bound of membrane performance (water flux) based on this zwitterion functionalized nanotube. Du et al. investigated hydration properties of carboxybetaine zwitterion brushes with varying separation distances between the quaternary ammonium cation and carboxylic anion.[44] They found that many factors influenced the hydration behaviors of the carboxybetaine brushes, including the values of both positive and negative charges, their separation distances and chain interactions. The

competition between the strong hydration of the charged groups and the dehydration of the hydrocarbon chains determines hydrophilic/hydrophobic tendency of the brushes. Various studies on interactions between zwitterions and organic matters have also been reported. For example, Shao et al. performed molecular simulations to study the interaction between carboxybetaine and chymotrypsin inhibitor 2 (a protein model)[47] and showed that the carboxybetaine doesn't preferentially accumulate near the protein surface. Using MD simulation, Nagumo et al. reported the free energy profiles of some amino acids approaching a zwitterionic monomer (a carboxybetaine derivative).[48] They found that these free energy profiles have almost no energetically remarkable minima, regardless of the type of amino-acid residues, indicating that this carboxybetaine derivative has an excellent antifouling property.

In our recent molecular simulation studies, we have investigated the antifouling property of PEG-grafted polyamide membrane.[52] We found that PEG coating can hold a tightly bound hydration water layer. When the alginate gel is dragged to approach the PEG coating surface, a strong repulsive hydration force is observed due to the compression of this hydration layer. We have also studied the effect of the PEG coverage on the membrane−foulant interactions and found that the alginate gel has a strong tendency to drift to the uncovered polyamide membrane surface.

Following this simulation study, we present our recent work on the hydration behavior of a sulfobetaine coating and its antifouling properties. This is an extensively studied antifouling material in many membrane fouling experiments.[19-21] Initially, we will study the ion-pairing behaviors of sulfobetaine zwitterions by an umbrella sampling technique[53, 54]. We will then investigate the different hydration structural properties of

sulfobetaine brush array at different grafting densities. This is followed by the simulation studies of foulant-sulfobetaine coating interactions and the effect of grafting density on its antifouling mechanism.

2. MOLECULAR MODELS AND SIMULATION METHODS

2.1. Molecular Models

2.1.1. Sulfobetaine Brush. Several methods have been developed for grafting zwitterionic molecules on a polyamide membrane surface, leading to different zwitterionic brush structures. In this work the sulfobetaine brush model is based on the click chemistry used by Yu et al.[20] An alkyne-PZ was first synthesized using reversible additional-fragmentation, chain-transfer radical polymerization. Polyamide membrane was then functionalized with azide functional groups through bromination of amide groups, and subsequently S_N2 nucleophilic substitution of Br with azide functional groups. Finally, the alkyne-PZ was grafted onto azide-polyamide surface by an azide–alkyne cycloaddition click reaction. This process is illustrated in Figure 1a.

Our main purpose is to investigate the conformation of the sulfobetaine brush array (coating) and its interaction with foulant molecules in aqueous environment. In order to focus on the major molecular interactions and save computing time, several assumptions and simplifications are made. *First*, we only consider short sulfobetaine brushes with each "tree" containing five sulfobetaine branches (see Figure 1a.). Long sulfobetaine brushes with tens to hundreds of zwitterionic monomers branches certainly adopt different molecular conformation,[55] which is beyond current study. *Second*, the

grafting density in experiments often refers to the total quantity of grafting materials per unit area and has no direct correlation to the number density of brushes. However, in computational simulations, we only consider short sulfobetaine brushes. Therefore, we use the number density to define the low-, intermediate- and high-grafting densities of sulfobetaine brushes on a membrane surface. *Third*, we assume that polyamide membrane underneath the sulfobetaine coating plays a less important role in foulant-sulfobetaine coating interactions, thus polyamide membrane surface is not explicitly modeled in this simulation. We use two saturated benzene rings (see figure 1a and figure 2) to represent the root of the brush and the polyamide membrane. Further, in order to compare with previous simulation work,[45-47, 51] two -CH_2- groups are arranged between the sulfonate and quaternary ammonium groups in a sulfobetaine branch.

The simulation system is prepared by setting the sulfobetaine brushes evenly in a squared grid. Three grafting densities are considered as shown in Table 1. Configurational-bias Monte-Carlo sampling[56] is performed to sample the initial configurations. This technique allows for all brush conformations generated with the correct Boltzmann weight.[57] A total of 5100 water molecules are added to the simulation system to hydrate the sulfobetaine brush array, after 2ns MD equilibration run.

Table 1. Geometric Parameters Related to Different Grafting Densities of Sulfobetaine Brush Array

	number of sulfobetaine brushes	area per brush	distance between brushes
low density	9	3.24 nm^2	1.8 nm

intermediate density	9	1.44 nm^2	1.2 nm
high density	16	0.64 nm^2	0.8 nm

2.1.2. Foulant. As in our previous simulation study,[52] we select alginate as the foulant model because this type of molecules are widely found in the environment and believed to be the major contributor to the organic fouling.[58] Alginate contains β-D-(1→4)-mannuronic acid (**M**) and α-L-(1→4)-guluronic acid (**G**) residues. In this work, only **G** residues are considered due to its specific spacing and geometry of the carboxylate functional groups for cation binding.[59] A detailed molecular structure of alginate is given in Figure 1b. All the carboxyl groups in the G residue are assumed deprotonated under the neutral pH condition,[60] considering the acid-dissociation-constant (pKa) of alginic acid is between 3.38 - 3.65.[61] A total of 12 sodium ions are added to compensate the 12 $–COO^-$ groups in the 4 alginate chains in the simulation system.

Alginate gel consisting of 4 alginate chains is made by adding 10 calcium ions (Ca^{2+}) and 20 chloride co-ions (Cl^-) through calcium binding in a solution system, containing 3500 water molecules. This subsystem is eventually combined with the previously built sulfobetaine brush array system, yielding a 0.1M $CaCl_2$ solution.

2.2. Simulation Methods

2.2.1. Umbrella Sampling. The umbrella sampling method is used to determine the free energy profile between two sulfobetaine zwitterions or between two sulfobetaine brushes in different media.[53, 54] A single collective variable, the center of mass (COM) distance, *r*, between two molecules, is used for calculations. We calculate the free energy

profile $G(r) = -k_B T \ln[P(r)]$ + constant, where k_B is the Boltzmann's constant, T is the temperature, and $P(r)$ is the probability distribution of distance r obtained in the simulation. During the umbrella sampling, the trajectory is divided into N independent simulation segments with a constrained potential applied (the so-called the umbrella potential). A biased distribution of segment i, $P(r_i)$, is first obtained, followed by reconstruction of the unbiased distribution through histogram reweighting methods.[53, 54] Finally a continuous profile of $G(r)$ is obtained. The free energy calculated in this way reflects the realistic equilibrium property of the system. Detailed parameters for umbrella sampling will be given in Section 3.1.

2.2.2. MD simulation. MD simulations are carried out to study the equilibrium properties of sulfobetaine brush arrays and the interactions between the alginate gel and the sulfobetaine coating in an aqueous solution. The detailed simulation methods have been discussed in our previous publications.[62, 63] We use the LAMMPS computational package for all of the MD simulations.[64] Periodic boundary conditions are applied in the three directions. We use the OPLS all-atom force field[65, 66] to describe the interatomic interactions among the alginate gel and sulfobetaine arrays. This force field has been parameterized for most of the organic molecules in solutions. For sulfobetaine molecules, we use the partial charges developed by Shao et al. from the DFT calculations using the B3LYP/6-31G** functional and basis set.[46] The flexible simple point charge (SPC) water model[67, 68] is employed in MD simulations. We use the Aqvist SPC water compatible potentials[69] for the monovalent Na^+ and divalent Ca^{2+} ions. As the Aqvist's parameters are only available for alkali and alkaline-earth metal cations, we choose the potential parameters for halide Cl^- ion developed by Joung et al.[70] The particle-particle-particle-

mesh solver is used to calculate the long-range electrostatic interactions.[71] The cut-off distance for the short-range Lennard-Jones interactions is set to 10 Å. The equations of motion of the particles are propagated through the velocity Verlet algorithm with a time step of 1 fs in a constant-*NVT* ensemble. The temperature is controlled at 300 K using the Nose-Hoover thermostat.

Figure 2 shows an equilibrium snapshot of the molecular simulation system, in which the hydrated sulfobetaine brush array at the high grafting density and an alginate gel are immersed in water. The sulfobetaine brush coating has a thickness around 3.6 nm. The Ca^{2+} alginate gel is right above the sulfobetaine array. Water layers on the two sides of the coating have a thickness around 10 nm (upper) and 4 nm (lower), respectively. A vapor phase of about 20 nm above the upper solution phase (not shown in Figure 2) is introduced into the system.[63] This arrangement allows the system pressure to be comparable to the water vapor pressure.[72]

3. RESULTS

3.1. Ion-pairing Behaviors of Sulfobetaine Zwitterions and Sulfobetaine Brushes by Free Energy Calculations

A sulfobetaine zwitterion contains two oppositely charged functional groups, the sulfonate group that carries a negative charge and the quaternary ammonium group that carries a positive charge. Thus noncovalent bond due to electrostatic interactions can be formed.[73-78] For this type of electrostatic "ion-paring" interaction, we are particularly interested in its strength in different solvent media. Here, we use the umbrella sampling technique[53, 54, 79] to calculate free energy changes versus the distance between two

sulfobetaine zwitterions (Figure 3) or between two sulfobetaine brushes (Figure 5) in different media. For each case, three independent *NVT* MD simulations are performed at T = 300K in (1) vacuum, (2) water, and (3) 0.5M NaCl solution. In the sulfobetaine zwitterion case, a total of 20 umbrella intervals are set between the two sulfobetaine zwitterions, whose center of mass (COM) distance varies from 3 Å to 13 Å. In the sulfobetaine brush case, a total of 26 intervals between 7 Å and 20 Å COM distance are used. The COM distance between the two sulfobetaine zwitterions or brushes are restrained by a harmonic spring with a spring constant of 20 kJ/(mol-Å^2). Umbrella sampling of molecular configuration is carried out by gradually changing the equilibrium distance of the spring within each interval of 0.5 Å. The simulation time for each bin is 2 ns.

Figure 4a shows the free energy changes versus the COM distance between two zwitterions in the three media. The free energy value with large distance of COM (i.e. 11 Å for Figure 4a and 19 Å for Figure 4b) is set as the reference. It is seen that the free energy profile in vacuum is significantly different from that in water or in NaCl solution. In vacuum, the profile exhibits a global minimum at about 4.5Å and a second minimum at about 8.5 Å. The energy barrier between the two is around 30 kJ/mol. The equilibrium configuration of the two sulfobetaine zwitterions at the global minimum is shown in Figure 3a, in which two sulfonate-ammonium ion pairs are formed, characterized by the N-S distance between 4.3 – 4.4Å. The first energy barrier between 4.5Å and 8.5Å shown in Figure 4a corresponds to the energy to dissociate the first ion pair, while the second energy barrier corresponds to the complete detachment of the two zwitterions.

The free energy profiles of the two sulfobetaine zwitterions in water and NaCl solution are very similar. Figure 4a shows a very small energy barrier around 0.5 kJ/mol at about 5.3Å, indicating a negligible free energy change during the dissociation of the zwitterion pair. Molecular configuration shows that the ion pair between the two zwitterions are essentially hydrated and separated by water molecules at the local free energy minimum at about 5Å (point C in Figure 4a). This ion-pair structure is far less stable than that in vacuum. Moreover, only one hydrated, weakly bound ion pair (Fig.3c) is infrequently observed, characterized by the N-S distance around 4.46Å. Thus it is more energetically favorable for the two sulfobetaine zwitterions being fully hydrated rather than forming ion-pair in water or in 0.5M NaCl solution. Our results are consistent with previous simulation results in which no aggregation of sulfobetaine zwitterions was observed in solutions.[45, 46]

Figure 4b shows the free energy changes versus the COM distance between two zwitterion brushes in the three media. The model of sulfobetaine brush is described in section 2.1.1. Notably, the free energy profiles for the two zwitterion brushes are quite different from those for the two zwitterion pairs. In vacuum, the free energy minima for the two zwitterion brushes exhibit a flat region between 11 – 14Å COM distances. The equilibrium configuration of the two sulfobetaine brushes within this region is shown in Figure 5a, corresponding to point D in Figure 4b. Here, there are two types of sulfonate-ammonium ion pairs identified. The first type is the intra ion pair from the same sulfobetaine brush (the purple dashed lines), and the second type is the inter ion pair between the two sulfobetaine brushes (the blue dashed lines). The bond lengths of these ion pairs (N-S distance) vary from 4.7 to 5.2 Å. When the two brushes are gradually

pulled apart in the region of 11-14 Å COM distances, all ion pairs are kept intact through the internal adjustments of branches in sulfobetaine brushes, resulting in negligible free energy changes in this region. The energy barrier of ~18 kJ/mol between the COM distances 14-15 Å is attributed to overcoming the van der Waals (vdw) and electrostatic interactions between the two brushes, especially between the two adjacent branches in their own sulfobetaine brushes that are suddenly separated during the internal adjustments, as shown in Figure 5a and 5b. The next energy barrier of ~30 kJ/mol from 17 to 18.5Å, as shown in Figure 4b, corresponds to the energy to dissociate the first inter ion pair. Molecular configuration corresponding to this first dissociation is shown in Figure 5c, and the new free energy level is denoted by point F in Figure 4b. This dissociation barrier is consistent with the ion pair dissociation between the two sulfobetaine zwitterions (see Figure 4a).

The free energy profiles of sulfobetaine brushes in water and in 0.5M NaCl solution exhibit a similar trend, as shown in Figure 4b. They both have energy minima at about 9.4 Å distance, followed by an energy ramp during the dissociation. Molecular configurations at the free energy minima are shown in Figure 5d and 5e, corresponding to points G and H in Figure 4b. Here, ion pairs between the two sulfobetaine brushes in both media are rarely observed, and only few intra ion pairs are seen occasionally (the purple dashed line in Figure 5d and 5e). The fully hydrated state of zwitterion branches leads to a much extended structure of sulfobetaine brushes (see section 3.3 discussion). An important question concerns why the energy ramp beyond 9.5Å in water is higher by approximately 5-10 kJ/mol than that in NaCl solution. To understand this, we show in Figure 5e all the ions within 5Å distance from the sulfobetaine brushes. It is clearly seen

that these ions coordinate with the oppositely charged functional groups, such as Na^+ ions around the sulfonate groups and Cl^- co-ions around the quaternary ammonium groups. Although these ionic bindings are dynamic and not stable, they impose a screening effect on the local charges of sulfobetaine branches; therefore reducing the long range electrostatic interactions in the salt solution, and resulting in a low free energy barrier during dissociation. Interestingly, it has been reported that the solubility of sulfobetaine derivatives increases significantly in high-concentration salt solutions,[80, 81] which is consistent with our free energy calculations.

3.2. Hydration Structure of Sulfobetaine Brush Array

Figure 6 shows representative molecular configurations of hydrated sulfobetaine brush arrays with different grafting densities. At the high grafting density, the brushes tend to self-assemble into a vertically aligned structure; while at the low grafting density, they are randomly oriented and fully hydrated by water molecules with very weak ion-pair interactions. Figure 7 shows the density distributions of sulfobetaine brush arrays and water, as well as other specific elemental groups in the zwitterions. The water-zwitterion array boundary is defined as the distance at which the density of water molecules is about 80% of its bulk value. Accordingly, we estimate the thicknesses of the high, intermediate and low grafting density brush arrays are 3.6, 2.7, and 1.7 nm, respectively. The averaged material densities of the three brush arrays are 1.1, 0.5, and 0.35 g/cm^3, respectively. The different hydration structures of brush arrays with different material densities lead to the changes of their surface chemistry. For example, the high-grafting-density brush array exposes more sulfonate groups at the water-zwitterion

interface than the low-grafting-density brush array does, resulting in a high-density negatively charged sulfonate groups remaining on the surface and the positively charged quaternary ammonium groups (the blue N group in Figure 7a) staying largely in the inner region of the brush array. This shows that at the water-zwitterion coating interface, the high-density brush array is negatively charged, while the low-density brush array tends to be a neutral surface.

In order to further study the detailed hydration structure of zwitterion brush array at different grafting density, in Figure 8a-c, we plot the radial distribution functions (RDFs) for different contact pairs. The corresponding integrals of these RDFs, the coordination numbers, are shown in Figure 8d-f. In particular, we investigate the hydration property of C atoms in the quaternary ammonium group by looking at the C (quaternary ammonium) – O (water) RDF profile and its integration with distance, because the central N atom is far away from the surrounding water molecules. Similarly, for the sulfonate group, we calculate the O (sulfonate) – O (water) RDF profile and its integration to characterize its hydration property. In Figure 8a, the first and second hydration shells of the O atom in sulfonate groups are located at about 2.7 Å and 5 Å, regardless of the grafting density. In contrast, Figure 8b shows different shifts of RDF peaks of the C (quaternary ammonium) – O (water) contact pair depending on the grafting density. For the high grafting density array, the first hydration peak is located at about 3.1 Å. This first peak is shifted by 0.5 Å for the intermediate- and low-grafting densities. The similar shifts are also seen for the second hydration peaks. We attribute this difference in RDF shift between the O (sulfonate) – O (water) and C (quaternary ammonium) – O (water) to the different interaction strengths between the quaternary

ammonium-water and sulfonate–water contact pairs. Namely, the quaternary ammonium-water interaction is much weaker than the sulfonate-water interaction. Consequently, the hydration shells around the quaternary ammonium groups are more favorable to deform under more constraint conditions (i.e. in high-grafting-density array) than the hydration shells around sulfonate groups. These findings are consistent with Shao et al.'s simulation results, which show that water molecules around the sulfonate groups have a higher structure order and a lower mobility than those around quaternary ammonium groups.[46]

To investigate ion pair interactions, Figure 8c shows the O (sulfonate) – C (quaternary ammonium) RDFs for three different grafting densities. Note that the distance between the quaternary ammonium C atoms and the sulfonate O atoms *within* the same sulfobetaine zwitterion branch is in the range of 5 – 6 Å, while the distance between the two in an ion pair is about 3 – 3.5 Å. Figure 8c and 8f clearly shows the existence of ion pairs whose total number increases with the grafting density. About 3 quaternary ammonium C atoms coordinate with one sulfonate O in the high-grafting-density array, while less than 0.5 in the low-grafting-density array.

Figure 8d shows the coordination numbers of water molecules around the oxygen atoms in sulfonate groups. These functional groups in the high-grafting-density array are less hydrated than in the low-grafting-density array. Here, only 1.6 water molecules are within the first hydration shell of sulfonate in the high-grafting-density array, while in the low-grafting-density array this number of hydration water molecules is increased to 2.3. In Shao el al.'s paper,[46] the sulfonate groups have a coordination number of 7.08 water molecules within the first hydration shell in a fully hydrated state, namely, about 2.36 water molecules around the O atoms in a sulfonate group. Our calculation result for the

low-grafting-density array is close to their simulation result, indicating that the low-grafting-density array of sulfobetaine brushes is almost fully hydrated. The overall inadequate hydration for the high-grafting-density array is also illustrated in Figure 7a, which shows that the average water density within the brush array is only about 0.2 g/cm^3.

3.3. Repulsive Hydration Force between Alginate Gel and Sulfobetaine Brush Array

In order to understand the antifouling mechanism of sulfobetaine zwitterion coating, we carried out steered molecular dynamics (SMD) simulations to study molecular interactions between the brush array and an alginate foulant in an aqueous solution. While the umbrella sampling can be used to find the realistic free energy of the alginate gel on the surface at different locations, the computational cost is enormous. For this reason, we follow our previous work by simply dragging the alginate foulant towards the zwitterion coating surface at different locations. While this method is a very approximate approach to detect foulant-surface interactions, it can significantly save computing times. After a 5 ns MD equilibrium run, no attachment of the alginate gel on the sulfobetaine array is seen, indicating that no strong attractive force exists between the foulant and the coating surface. This is similar to what we found for PEG coating,[52] but differs from the case of polyamide membrane surfaces, in which we observed strong ionic binding between an alginate gel and the membrane surface.[62, 63] We choose nine different locations shown in Figure 9 to run SMD simulations. The alginate gel is pushed downward to the sulfobetaine brush array by a driving spring without any constraint in the lateral directions. The driving speed is 0.005 Å/ps, slow enough to ensure an approximately quasistatic approaching to the surface. For each grafting density brush

array, no significant differences in the force-distance curves is seen for the nine independent SMD runs. Thus only one force-distance curve from the nine simulations at each brush array density is chosen for analysis. These force-distance curves at different brush array densities are shown in Figure 10. Note that repulsive forces in simulations correspond to negative values, while adhesion forces correspond to positive values. These are consistent with our previous definitions.[62, 63] In all three SMD simulations, repulsive forces are seen to increase dramatically as the alginate gel is dragged to press the zwitterion brush array. However, the distance at which the repulsive force begins to dramatically increase depends on the grafting density. The repulsive force corresponding to the high-density array starts to increase much earlier and steeper, mainly because of the denser and thicker zwitterion coating material. This phenomenon can be further analyzed by looking at the different deformation mechanisms of sulfobetaine branches under compression. We use three angles θ_{xy}, θ_{xz} and θ_{yz} to quantify the orientation of each branch in brushes. θ_{xy} is defined as the angle between the projection of vector **R** on the *x*-*y* plane and the *y*-axis (see Figure 1c); vector **R** is defined from the C atom connecting to the backbone of the brush to the S atom in the sulfonate group. These two atoms are highlighted in purple in Figure 1a the middle panel, which shows a typical branch. θ_{xz} and θ_{yz} follow the similar definition as θ_{xy}, but as they both have the similar distribution as θ_{xy} during the deformation of the brush array, we only focus on θ_{xy} orientation distribution changes. The histograms of θ_{xy} in an equilibrium run over 2 ns are shown in Figure 11a. It is seen that the grafting density influences the orientations of branches: θ_{xy} of the high-grafting-density array takes two major values around $-\pi$ and π due to the less hydrated, more organized structure of the self-assembled brush array, while θ_{xy} is more evenly

distributed in the low-grafting-density array due to its fully hydrated, randomly oriented structure.

When the alginate gel approaches the sulfobetaine array surface, the surface coating is under compression. Figure 11b shows the redistributions of orientation angle θ_{xy} of the three brush arrays under the same load of 1 nN, corresponding to the load points A, B and C in the three force-distance curves shown in Figure 10. Negligible changes of θ_{xy} distribution are seen for the high-grafting-density array, and dramatic changes of θ_{xy} are seen for the intermediate- and low-grafting-density arrays. We attribute this θ_{xy} re-distribution to the flexibility of zwitterion branches. In Figure 12 we show the molecular configurations of the high- and intermediate (as the low-density array has the similar behavior as the intermediate array, we only show the latter)-grafting-density arrays under 1 nN compression. Compared with the high-density array configuration, the change in molecular configuration of the intermediate-density array under 1 nN force is significant, resulting in a large cavity on the surface coating to accommodate the alginate gel. We further investigate changes of the number of water molecules within a 3Å layer around the van der Waals (vdw) surface of sulfobetaine array. We find that under the compression of alginate gel, water molecules around the high-density array is only reduced from 150 ±5 to 148±8, indicating that the surface water is difficult to be squeezed out and thus the repulsive force mainly originates from compressing the densely populated hydration water between the gel and sulfobetaine array (Figure 12a). This situation is very similar to our previous findings for the PEG coating.[52] For the intermediate-grafting-density array whose surface morphology has a large change under alginate compression, water molecules around the vdw surface is reduced from 188±12

to 169 ± 18. We find that the repulsive force is mainly due to the deformation of zwitterion branches, namely, the change of the configurational entropy of the brush array. Although there is still a hydration water layer around the array surface, these hydration water molecules have less contribution to the repulsive force. This conclusion can be verified in Figure 10, in which we show the hydration water layer-foulant interactions during SMD simulations for the high-, intermediate- and low-grafting-density array surfaces. The significantly monotonic increase of alginate gel-water interaction can only be observed in the high density system. In contrast, force fluctuations around zero between alginate gel and water layer are observed in the intermediate- or low-grafting density systems, indicating that compression of hydration water layer has much less contribution to the total repulsive force. Specifically, for the low-grafting-density array, we find that several branches are heavily twisted under compression. Note that even the space between the two brushes in this case is as wide as 18 Å, which is much larger than the average diameter of the alginate gel of ~ 8 Å, there is still strong repulsive force due to the deformation and distortion of zwitterion branches.

4. SUMMARY

In this study, we perform molecular dynamics simulations to investigate the interactions between two sulfobetaine zwitterions and between two sulfobetaine brushes. Simulation results show that it is more energetically favorable for the two sulfobetaine zwitterions or brushes being fully hydrated in aqueous solutions than in vacuum where strong ion pairs are formed. The energy barriers for dissociation in water and solution are much lower than that in vacuum. In addition, the energy ramp in water is higher by

approximately 5-10 kJ/mol than that in NaCl solution, possibly due to ion screening effect. Three sulfobetaine brush arrays with different grafting densities have been built to investigate the interactions between foulant gel and sulfobetaine coating in aqueous environment. The different properties of each array, including the thickness, distribution of functional groups, hydration structure and the branch orientations have been carefully studied. The SMD simulations reveal strong repulsive forces between foulant gel and sulfobetaine array surface regardless of grafting densities, indicating their good antifouling properties. We also show the different origins of these repulsive forces: in high-grafting-density array, the major contributor is the surface hydration layer, while deformation of surface branches has main contribution in the intermediate and low-density arrays. The present study provides detailed information on the hydration structure and antifouling mechanisms of sulfobetaine coating from the molecular perspectives. These findings may help to understand general antifouling mechanisms of various polyzwitterion coatings using different grafting materials and methodology, and shed light on the molecular design of future anti-fouling materials.

ACKNOWLEDGEMENTS

This work was supported by the National Science Foundation (NSF 1034158 and NSF 1149704), American Chemical Society Petroleum Research Fund (ACS PRF), and the National Energy Research Scientific Computing Center (NERSC).

1. Elimelech, M.; Phillip, W. A., The Future of Seawater Desalination: Energy, Technology, and the Environment. *Science* **2011,** 333, (6043), 712-717.
2. Elimelech, M., The global challenge for adequate and safe water. *Journal of Water Supply Research and Technology-Aqua* **2006,** 55, (1), 3-10.

3. Shannon, M. A.; Bohn, P. W.; Elimelech, M.; Georgiadis, J. G.; Marinas, B. J.; Mayes, A. M., Science and technology for water purification in the coming decades. *Nature* **2008,** 452, (7185), 301-310.
4. Khulbe, K. C.; Feng, C.; Matsuura, T., The Art of Surface Modification of Synthetic Polymeric Membranes. *Journal of Applied Polymer Science* **2010,** 115, (2), 855-895.
5. Camacho, L. M.; Dumee, L.; Zhang, J.; Li, J.-d.; Duke, M.; Gomez, J.; Gray, S., Advances in Membrane Distillation for Water Desalination and Purification Applications. *Water* **2013,** 5, (1), 94-196.
6. Zhao, S.; Zou, L.; Tang, C. Y.; Mulcahy, D., Recent developments in forward osmosis: Opportunities and challenges. *J. Membr. Sci.* **2012,** 396, 1-21.
7. Kang, G.-d.; Cao, Y.-m., Development of antifouling reverse osmosis membranes for water treatment: A review. *Water Research* **2012,** 46, (3), 584-600.
8. Lee, K. P.; Arnot, T. C.; Mattia, D., A review of reverse osmosis membrane materials for desalination-Development to date and future potential. *J. Membr. Sci.* **2011,** 370, (1-2), 1-22.
9. Tang, C. Y.; Chong, T. H.; Fane, A. G., Colloidal interactions and fouling of NF and RO membranes: A review. *Advances in Colloid and Interface Science* **2011,** 164, (1-2), 126-143.
10. Li, D.; Wang, H., Recent developments in reverse osmosis desalination membranes. *J. Mater. Chem.* **2010,** 20, (22), 4551-4566.
11. Milton Harris, J., *Poly(ethylene glycol) chemistry: biotechnical and biomedical applications*. Springer Science+Business Media: New York, 1992.
12. Zhang, Z.; Chao, T.; Chen, S. F.; Jiang, S. Y., Superlow fouling sulfobetaine and carboxybetaine polymers on glass slides. *Langmuir* **2006,** 22, (24), 10072-10077.
13. Vaisocherova, H.; Yang, W.; Zhang, Z.; Cao, Z. Q.; Cheng, G.; Piliarik, M.; Homola, J.; Jiang, S. Y., Ultralow fouling and functionalizable surface chemistry based on a zwitterionic polymer enabling sensitive and specific protein detection in undiluted blood plasma. *Anal. Chem.* **2008,** 80, (20), 7894-7901.
14. Yang, W.; Zhang, L.; Wang, S. L.; White, A. D.; Jiang, S. Y., Functionalizable and ultra stable nanoparticles coated with zwitterionic poly(carboxybetaine) in undiluted blood serum. *Biomaterials* **2009,** 30, (29), 5617-5621.
15. Yang, W.; Chen, S. F.; Cheng, G.; Vaisocherova, H.; Xue, H.; Li, W.; Zhang, J. L.; Jiang, S. Y., Film thickness dependence of protein adsorption from blood serum and plasma onto poly(sulfobetaine)-grafted surfaces. *Langmuir* **2008,** 24, (17), 9211-9214.
16. Zhang, Z.; Chen, S. F.; Chang, Y.; Jiang, S. Y., Surface grafted sulfobetaine polymers via atom transfer radical polymerization as superlow fouling coatings. *J. Phys. Chem. B* **2006,** 110, (22), 10799-10804.
17. Gaberc-Porekar, V.; Zore, I.; Podobnik, B.; Menart, V., Obstacles and pitfalls in the PEGylation of therapeutic proteins. *Curr. Opin. Drug Discov. Dev.* **2008,** 11, (2), 242-250.
18. Jiang, S.; Cao, Z., Ultralow-Fouling, Functionalizable, and Hydrolyzable Zwitterionic Materials and Their Derivatives for Biological Applications. *Advanced materials* **2010,** 22, (9), 920-932.
19. Yang, R.; Xu, J.; Ozaydin-Ince, G.; Wong, S. Y.; Gleason, K. K., Surface-Tethered Zwitterionic Ultrathin Antifouling Coatings on Reverse Osmosis Membranes by Initiated Chemical Vapor Deposition. *Chemistry of Materials* **2011,** 23, (5), 1263-1272.
20. Yu, H.-Y.; Kang, Y.; Liu, Y.; Mi, B., Grafting polyzwitterions onto polyamide by click chemistry and nucleophilic substitution on nitrogen: A novel approach to enhance membrane fouling resistance. *J. Membr. Sci.* **2014,** 449, 50-57.
21. Bernstein, R.; Belfer, S.; Freger, V., Bacterial attachment to RO membranes surface-modified by concentration-polarization-enhanced graft polymerization. *Environ Sci Technol* **2011,** 45, (14), 5973-80.
22. Mi, Y.-F.; Zhao, Q.; Ji, Y.-L.; An, Q.-F.; Gao, C.-J., A novel route for surface zwitterionic functionalization of polyamide nanofiltration membranes with improved performance. *J. Membr. Sci.* **2015,** 490, 311-320.
23. Zhang, Y.; Wang, Z.; Lin, W.; Sun, H.; Wu, L.; Chen, S., A facile method for polyamide membrane modification by poly(sulfobetaine methacrylate) to improve fouling resistance. *J. Membr. Sci.* **2013,** 446, 164-170.
24. Chang, Y.; Chang, W. J.; Shih, Y. J.; Wei, T. C.; Hsiue, G. H., Zwitterionic Sulfobetaine-Grafted Poly(vinylidene fluoride) Membrane with Highly Effective Blood Compatibility via Atmospheric Plasma-Induced Surface Copolymerization. *ACS Appl. Mater. Interfaces* **2011,** 3, (4), 1228-1237.
25. Chen, S. F.; Li, L. Y.; Zhao, C.; Zheng, J., Surface hydration: Principles and applications toward low-fouling/nonfouling biomaterials. *Polymer* **2010,** 51, (23), 5283-5293.

26. Schlenoff, J. B., Zwitteration: Coating Surfaces with Zwitterionic Functionality to Reduce Nonspecific Adsorption. *Langmuir* **2014,** 30, (32), 9625-9636.
27. Sun, Q.; Su, Y. L.; Ma, X. L.; Wang, Y. Q.; Jiang, Z. Y., Improved antifouling property of zwitterionic ultrafiltration membrane composed of acrylonitrile and sulfobetaine copolymer. *J. Membr. Sci.* **2006,** 285, (1-2), 299-305.
28. Yang, W. J.; Neoh, K. G.; Kang, E. T.; Teo, S. L. M.; Rittschof, D., Polymer brush coatings for combating marine biofouling. *Prog. Polym. Sci.* **2014,** 39, (5), 1017-1042.
29. Yang, Y. F.; Li, Y.; Li, Q. L.; Wan, L. S.; Xu, Z. K., Surface hydrophilization of microporous polypropylene membrane by grafting zwitterionic polymer for anti-biofouling. *J. Membr. Sci.* **2010,** 362, (1-2), 255-264.
30. Chen, S. F.; Zheng, J.; Li, L. Y.; Jiang, S. Y., Strong resistance of phosphorylcholine self-assembled monolayers to protein adsorption: Insights into nonfouling properties of zwitterionic materials. *J. Am. Chem. Soc.* **2005,** 127, (41), 14473-14478.
31. Jiang, S. Y.; Cao, Z. Q., Ultralow-Fouling, Functionalizable, and Hydrolyzable Zwitterionic Materials and Their Derivatives for Biological Applications. *Advanced materials* **2010,** 22, (9), 920-932.
32. Sin, M. C.; Chen, S. H.; Chang, Y., Hemocompatibility of zwitterionic interfaces and membranes. *Polym. J.* **2014,** 46, (8), 436-443.
33. Chang, Y.; Shih, Y. J.; Lai, C. J.; Kung, H. H.; Jiang, S. Y., Blood-Inert Surfaces via Ion-Pair Anchoring of Zwitterionic Copolymer Brushes in Human Whole Blood. *Adv. Funct. Mater.* **2013,** 23, (9), 1100-1110.
34. Hadidi, M.; Zydney, A. L., Fouling behavior of zwitterionic membranes: Impact of electrostatic and hydrophobic interactions. *J. Membr. Sci.* **2014,** 452, 97-103.
35. Rohani, M. M.; Zydney, A. L., Protein transport through zwitterionic ultrafiltration membranes. *J. Membr. Sci.* **2012,** 397, 1-8.
36. Leng, C.; Han, X. F.; Shao, Q.; Zhu, Y. H.; Li, Y. T.; Jiang, S. Y.; Chen, Z., In Situ Probing of the Surface Hydration of Zwitterionic Polymer Brushes: Structural and Environmental Effects. *J. Phys. Chem. C* **2014,** 118, (29), 15840-15845.
37. Ridgway, H. F.; Orbell, J.; Gray, S., Molecular simulations of polyamide membrane materials used in desalination and water reuse applications: Recent developments and future prospects. *J. Membr. Sci.* **2017,** 524, 436-448.
38. Wei, T.; Zhang, L.; Zhao, H. Y.; Ma, H.; Sajib, M. S. J.; Jiang, H.; Murad, S., Aromatic Polyamide Reverse-Osmosis Membrane: An Atomistic Molecular Dynamics Simulation. *J. Phys. Chem. B* **2016,** 120, (39), 10311-10318.
39. Harder, E.; Walters, D. E.; Bodnar, Y. D.; Faibish, R. S.; Roux, B., Molecular Dynamics Study of a Polymeric Reverse Osmosis Membrane. *J. Phys. Chem. B* **2009,** 113, (30), 10177-10182.
40. Nadler, R.; Srebnik, S., Molecular simulation of polyamide synthesis by interfacial polymerization. *J. Membr. Sci.* **2008,** 315, (1-2), 100-105.
41. Eslami, H.; Muller-Plathe, F., Molecular Dynamics Simulation of Water Influence on Local Structure of Nanoconfined Polyamide-6,6. *J. Phys. Chem. B* **2011,** 115, (32), 9720-9731.
42. Kotelyanskii, M.; Wagner, N. J.; Paulaitis, M. E., Building large amorphous polymer structures: Atomistic simulation of glassy polystyrene. *Macromolecules* **1996,** 29, (26), 8497-8506.
43. Hughes, Z. E.; Gale, J. D., A computational investigation of the properties of a reverse osmosis membrane. *J. Mater. Chem.* **2010,** 20, (36), 7788-7799.
44. Du, H. B.; Qian, X. H., The Hydration Properties of Carboxybetaine Zwitterion Brushes. *J. Comput. Chem.* **2016,** 37, (10), 877-885.
45. Shao, Q.; He, Y.; Jiang, S. Y., Molecular Dynamics Simulation Study of Ion Interactions with Zwitterions. *J. Phys. Chem. B* **2011,** 115, (25), 8358-8363.
46. Shao, Q.; He, Y.; White, A. D.; Jiang, S. Y., Difference in Hydration between Carboxybetaine and Sulfobetaine. *J. Phys. Chem. B* **2010,** 114, (49), 16625-16631.
47. Shao, Q.; He, Y.; White, A. D.; Jiang, S. Y., Different effects of zwitterion and ethylene glycol on proteins. *J. Chem. Phys.* **2012,** 136, (22), 6.
48. Nagumo, R.; Akamatsu, K.; Miura, R.; Suzuki, A.; Tsuboi, H.; Hatakeyama, N.; Takaba, H.; Miyamoto, A., Assessment of the Antifouling Properties of Polyzwitterions from Free Energy Calculations by Molecular Dynamics Simulations. *Ind. Eng. Chem. Res.* **2012,** 51, (11), 4458-4462.

49. Chan, W. F.; Chen, H. Y.; Surapathi, A.; Taylor, M. G.; Shao, X. H.; Marand, E.; Johnson, J. K., Zwitterion Functionalized Carbon Nanotube/Polyamide Nanocomposite Membranes for Water Desalination. *ACS Nano* **2013,** 7, (6), 5308-5319.
50. Nagumo, R.; Ito, T.; Akamatsu, K.; Miura, R.; Suzuki, A.; Tsuboi, H.; Hatakeyama, N.; Takaba, H.; Miyamoto, A., Molecular dynamics simulations for microscopic behavior of water molecules in the vicinity of zwitterionic self-assembled monolayers. *Polym. J.* **2012,** 44, (11), 1149-1153.
51. Shao, Q.; Jiang, S. Y., Influence of Charged Groups on the Properties of Zwitterionic Moieties: A Molecular Simulation Study. *J. Phys. Chem. B* **2014,** 118, (27), 7630-7637.
52. Xiang, Y.; Xu, R. G.; Leng, Y. S., Molecular Dynamics Simulations of a Poly(ethylene glycol)-Grafted Polyamide Membrane and Its Interaction with a Calcium Alginate Gel. *Langmuir* **2016,** 32, (18), 4424-4433.
53. Kumar, S.; Bouzida, D.; Swendsen, R. H.; Kollman, P. A.; Rosenberg, J. M., The Weighted Histogram Analysis Method for Free-Energy Calculations on Biomolecules .1. The Method. *J. Comput. Chem.* **1992,** 13, (8), 1011-1021.
54. Torrie, G. M.; Valleau, J. P., Non-Physical Sampling Distributions in Monte-Carlo Free-Energy Estimation - Umbrella Sampling. *J. Comput. Phys.* **1977,** 23, (2), 187-199.
55. Chang, Y.; Chang, Y.; Higuchi, A.; Shih, Y. J.; Li, P. T.; Chen, W. Y.; Tsai, E. M.; Hsiue, G. H., Bioadhesive Control of Plasma Proteins and Blood Cells from Umbilical Cord Blood onto the Interface Grafted with Zwitterionic Polymer Brushes. *Langmuir* **2012,** 28, (9), 4309-4317.
56. Siepmann, J. I., A Method for the Direct Calculation of Chemical Potentials for Dense Chain Systems. *Molecular Physics* **1990,** 70, (6), 1145-1158.
57. Frenkel, D.; Smit, B., *Understanding molecular simulation from algorithms to application*. Academic Press: San Diego, 1996.
58. Plazinski, W.; Rudzinski, W., Molecular modeling of Ca2+-oligo(alpha-l-guluronate) complexes: toward the understanding of the junction zone structure in calcium alginate gels. *Structural Chemistry* **2012,** 23, (5), 1409-1415.
59. Perry, T. D. I. V.; Cygan, R. T.; Mitchell, R., Molecular models of alginic acid: Interactions with calcium ions and calcite surfaces. *Geochimica Et Cosmochimica Acta* **2006,** 70, (14), 3508-3532.
60. Brown, T.; Eugene H LeMay, H.; Bursten, B.; Murphy, C.; Woodward, P., *Chemistry: The Central Science*. Prentice Hall: Boston, 2011.
61. Davis, T. A.; Volesky, B.; Mucci, A., A review of the biochemistry of heavy metal biosorption by brown algae. *Water Research* **2003,** 37, (18), 4311-4330.
62. Xiang, Y.; Liu, Y.; Mi, B.; Leng, Y., Hydrated Polyamide Membrane and Its Interaction with Alginate: A Molecular Dynamics Study. *Langmuir* **2013,** 29, (37), 11600-11608.
63. Xiang, Y.; Liu, Y.; Mi, B.; Leng, Y., Molecular Dynamics Simulations of Polyamide Membrane, Calcium Alginate Gel, and Their Interactions in Aqueous Solution. *Langmuir* **2014,** 30, (30), 9098-9106.
64. Plimpton, S., FAST PARALLEL ALGORITHMS FOR SHORT-RANGE MOLECULAR-DYNAMICS. *J. Comput. Phys.* **1995,** 117, (1), 1-19.
65. Jorgensen, W. L.; Maxwell, D. S.; TiradoRives, J., Development and testing of the OPLS all-atom force field on conformational energetics and properties of organic liquids. *J. Am. Chem. Soc.* **1996,** 118, (45), 11225-11236.
66. Kaminski, G. A.; Friesner, R. A.; Tirado-Rives, J.; Jorgensen, W. L., Evaluation and reparametrization of the OPLS-AA force field for proteins via comparison with accurate quantum chemical calculations on peptides. *J. Phys. Chem. B* **2001,** 105, (28), 6474-6487.
67. Berendsen, H. J. C.; Postma, J. P. M.; van Gunsteren, W. F.; Hermans, J., *Interaction models for water in relation to protein hydration*. D. Riedel Publishing Co.: Dordrecht, The Netherlands, 1981.
68. Teleman, O.; Jonsson, B.; Engstrom, S., A Molecular Dynamics Simulation of a Water Model with Intramolecular Degrees of Freedom. *Molecular Physics* **1987,** 60, (1), 193-203.
69. Aqvist, J., Ion Water Interaction Potentials Derived from Free-Energy Perturbation Simulations. *Journal of Physical Chemistry* **1990,** 94, (21), 8021-8024.
70. Joung, I. S.; Cheatham, T. E., Determination of alkali and halide monovalent ion parameters for use in explicitly solvated biomolecular simulations. *Journal of Physical Chemistry B* **2008,** 112, (30), 9020-9041.
71. Hockney, R. W.; Eastwood, J. W., *Computer Simulation Using Particles*. Taylor and Francis Group: London, U.K., 1988.

72. Leng, Y., Hydration Force between Mica Surfaces in Aqueous KCl Electrolyte Solution. *Langmuir* **2012,** 28, (12), 5339-5349.
73. Rybtchinski, B., Adaptive Supramolecular Nanomaterials Based on Strong Noncovalent Interactions. *ACS Nano* **2011,** 5, (9), 6791-6818.
74. Rehm, T. H.; Schmuck, C., Ion-pair induced self-assembly in aqueous solvents. *Chem. Soc. Rev.* **2010,** 39, (10), 3597-3611.
75. Rehm, T.; Stepanenko, V.; Zhang, X.; Wurthner, F.; Grohn, F.; Klein, K.; Schmuck, C., A new type of soft vesicle-forming molecule: An amino acid derived guanidiniocarbonyl pyrrole carboxylate zwitterion. *Org. Lett.* **2008,** 10, (7), 1469-1472.
76. Schmuck, C.; Wienand, W., Highly stable self-assembly in water: Ion pair driven dimerization of a guanidiniocarbonyl pyrrole carboxylate zwitterion. *J. Am. Chem. Soc.* **2003,** 125, (2), 452-459.
77. Rodler, F.; Linders, J.; Fenske, T.; Rehm, T.; Mayer, C.; Schmuck, C., pH-Switchable Vesicles from a Serine-Derived Guanidiniocarbonyl Pyrrole Carboxylate Zwitterion in DMSO. *Angew. Chem.-Int. Edit.* **2010,** 49, (46), 8747-8750.
78. Groger, G.; Stepanenko, V.; Wurthner, F.; Schmuck, C., Step-wise self-assembly of a small molecule with two orthogonal binding interactions leads to single stranded linear polymers in DMSO. *Chem. Commun.* **2009**, (6), 698-700.
79. Bonomi, M.; Branduardi, D.; Bussi, G.; Camilloni, C.; Provasi, D.; Raiteri, P.; Donadio, D.; Marinelli, F.; Pietrucci, F.; Broglia, R. A.; Parrinello, M., PLUMED: A portable plugin for free-energy calculations with molecular dynamics. *Comput. Phys. Commun.* **2009,** 180, (10), 1961-1972.
80. Sundaram, H. S.; Han, X.; Nowinski, A. K.; Ella-Menye, J. R.; Wimbish, C.; Marek, P.; Senecal, K.; Jiang, S. Y., One-Step Dip Coating of Zwitterionic Sulfobetaine Polymers on Hydrophobic and Hydrophilic Surfaces. *ACS Appl. Mater. Interfaces* **2014,** 6, (9), 6664-6671.
81. Zheng, S. X.; Yang, Q.; Mi, B. X., Novel antifouling surface with improved hemocompatibility by immobilization of polyzwitterions onto silicon via click chemistry. *Appl. Surf. Sci.* **2016,** 363, 619-626.

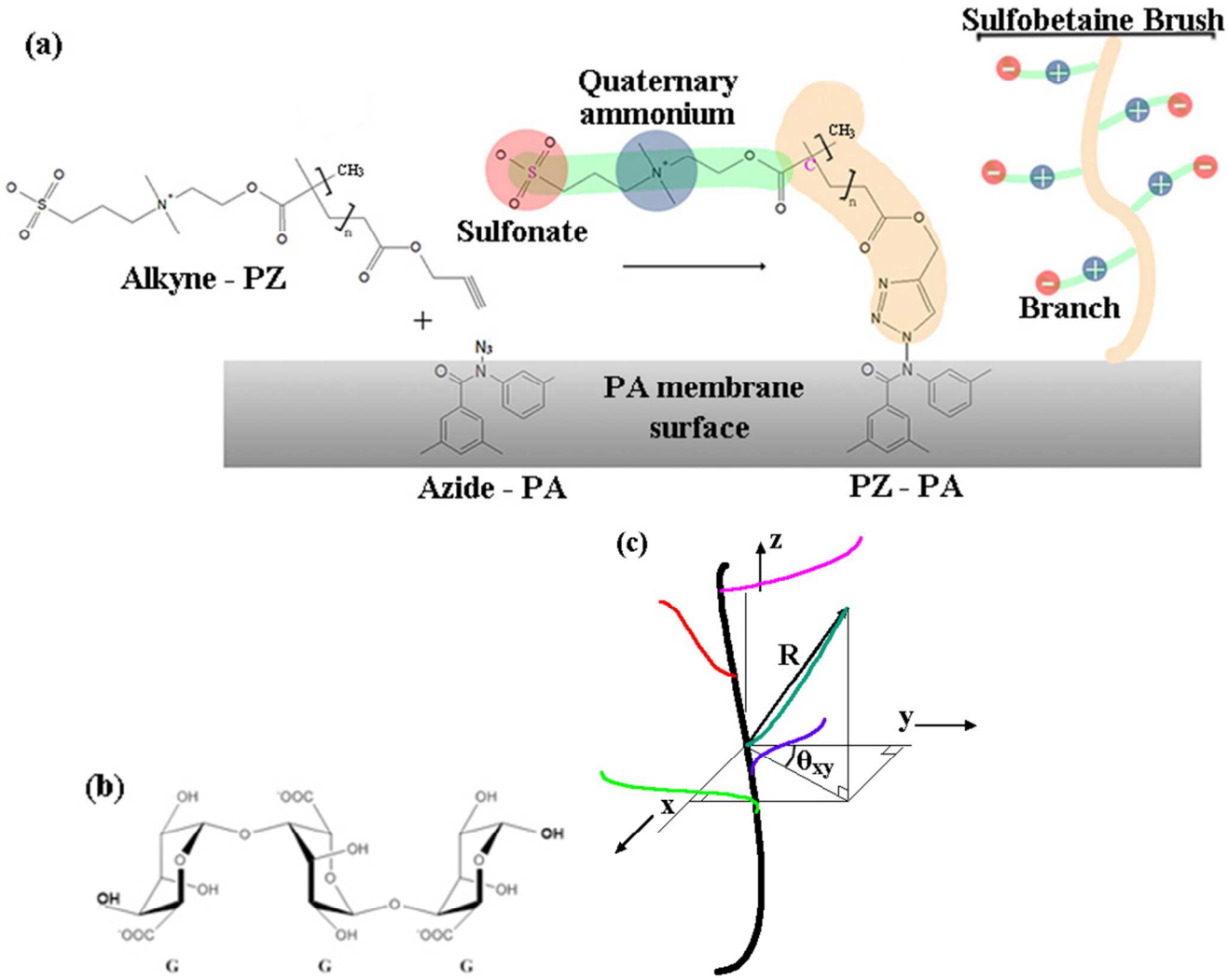

Figure 1. (a) The procedure of grafting sulfobetaine zwitterion on a polyamide membrane surface; (b) an alginate molecule that contains three L-guluronic acid (G) residues; (c) definition of θ_{xy} to evaluate the orientation of branches in a sulfobetaine brush.

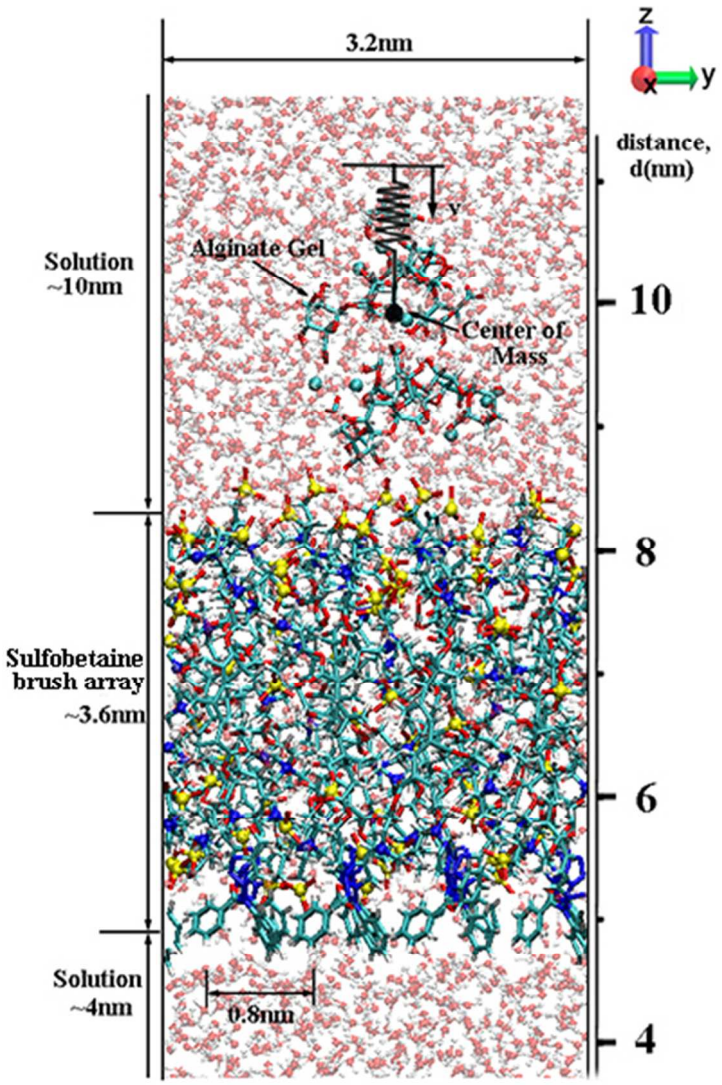

Figure 2. A snapshot of the simulation system containing sulfobetaine brush array with high grafting density and the alginate gel in solution. Colors in stick presentation: red, O; white, H; light blue, C; and dark blue, N. Colors in ball presentation in solution: light blue balls, Ca^{2+} ions. In order to illustrate the distribution of sulfonate groups and quaternary ammonium groups, all the S atoms in sulfonate groups are in yellow and all the N atoms in quaternary ammonium groups are in dark blue using ball presentation. A reference ruler for distance is indicated in the right of the diagram, which is used to evaluate the distance in Figure 7 and Figure 10. The saturated benzene rings representing the roots of brushes are located at 5nm distance along the z direction. A schematic of the SMD model applied to the alginate gel is also illustrated in the figure.

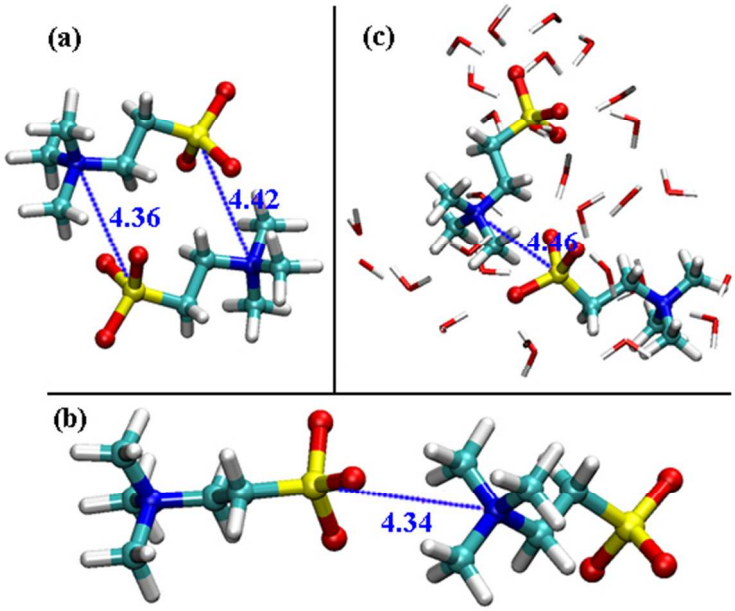

Figure 3. Ion pair structures between two sulfobetaine zwitterions. The S atoms in sulfonate functional groups are connected to the N atoms in quaternary ammonium groups with blue dashes lines. The distances between them are also illustrated. In vacuum, panel (a) shows two mutual ion pairs and panel (b) illustrates one single ion pair. Panel (c) shows a weakly bound ion pair structure in water. Water molecules close to this ion pair are also shown. Panel (a), (b) and (c) correspond to point A, B and C in Figure 4a, respectively. Colors: red, O; white, H; light blue, C; dark blue, N; and yellow, S.

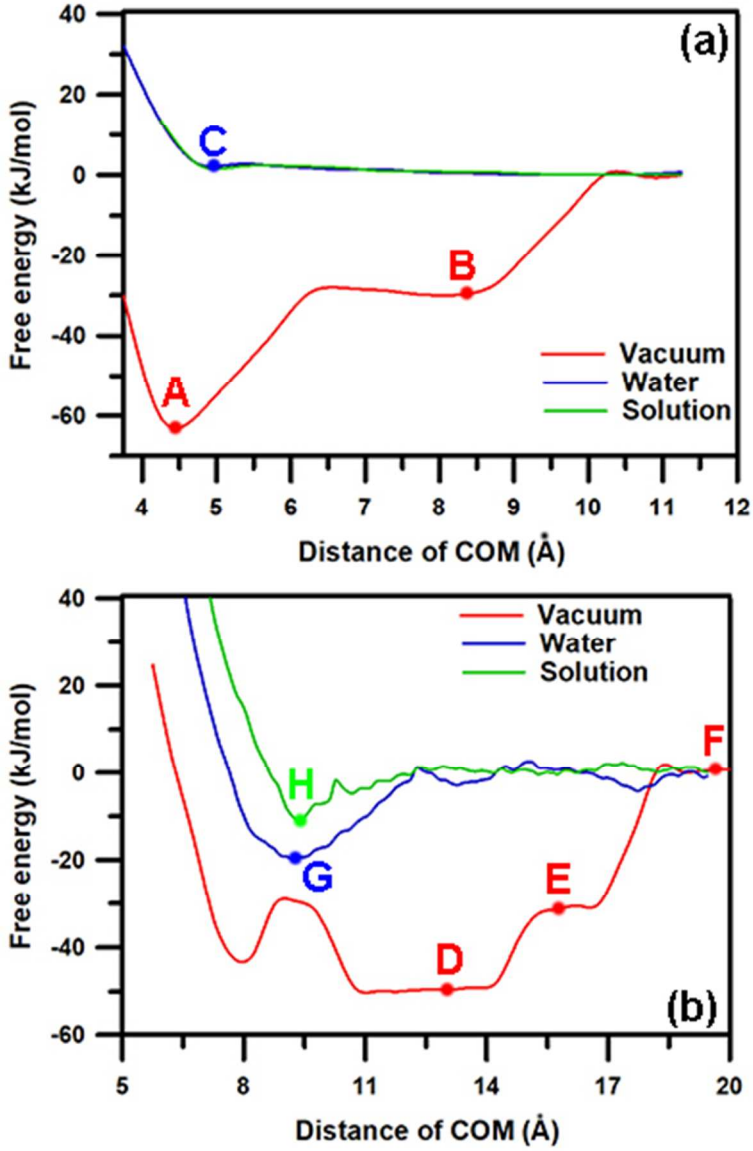

Figure 4. Free energy profiles of (a) two sulfobetaine zwitterions and (b) two sulfobetaine brushes in various media, calculated by umbrella sampling method. A single collective variable, the center of mass (COM) distance between two molecules, is used for calculations.

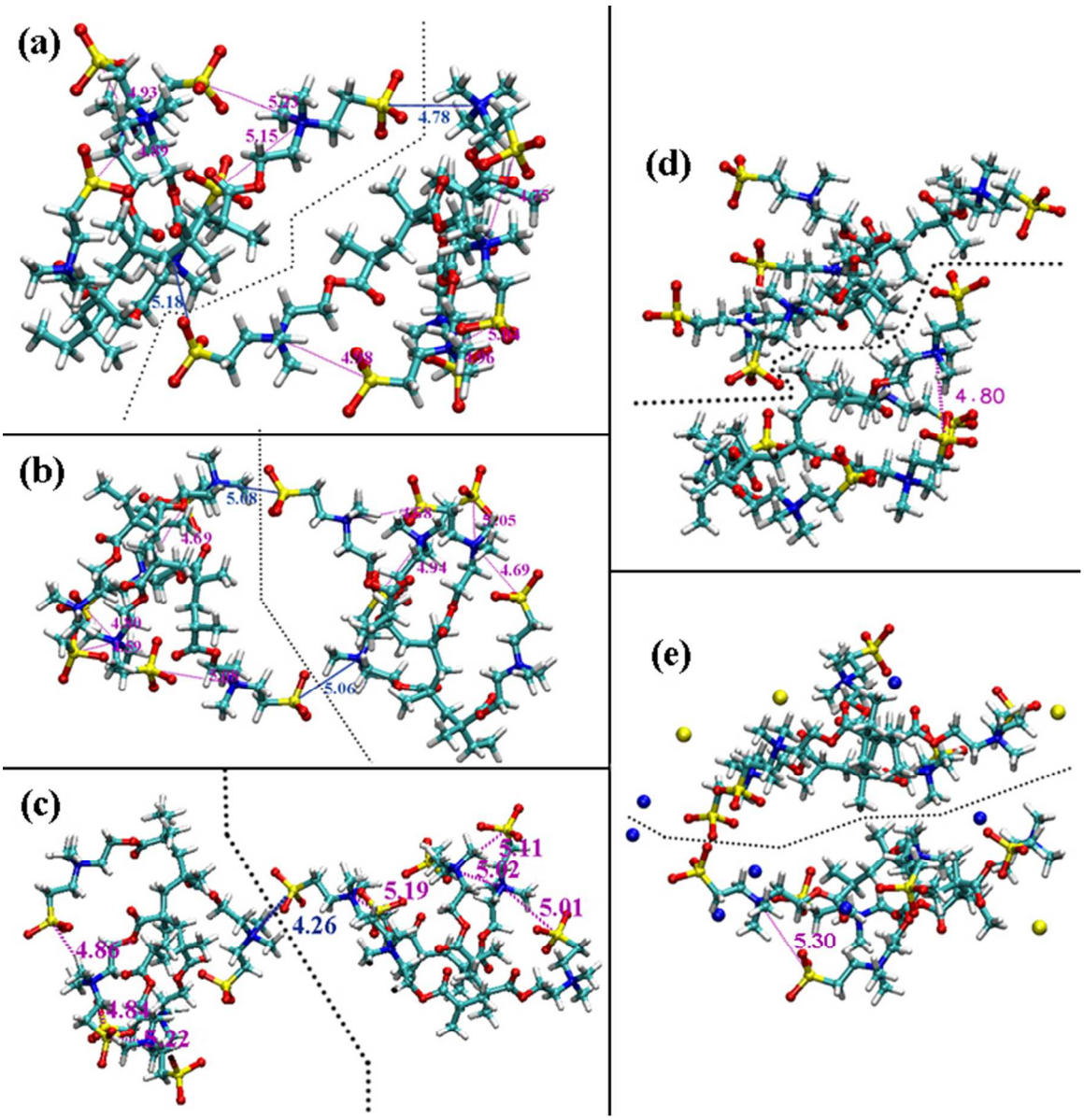

Figure 5. Typical ion pair structures between two sulfobetaine brushes. The S atoms in sulfonate functional groups are connected to the N atoms in quaternary ammonium groups with colorful dashes lines. The intra ion pairs are in purple and the inter ion pairs are in blue. The distances between them are also illustrated. Panels (a), (b) and (c) show pairs in vacuum. Panels (d) and (e) show brush structures in water and in NaCl solution, respectively. Panel (a), (b), (c), (d) and (e) correspond to point D, E, F, G and H in Figure 4b, respectively. Two brushes are separated by black dashes lines in order to be distinguished. Colors in stick presentation: red, O; white, H; light blue, C; dark blue, N; and yellow, S. Colors in ball presentation in solution: dark blue, Na^+; and yellow, Cl^-. Water molecules in (d) and (e) are not shown for clarity.

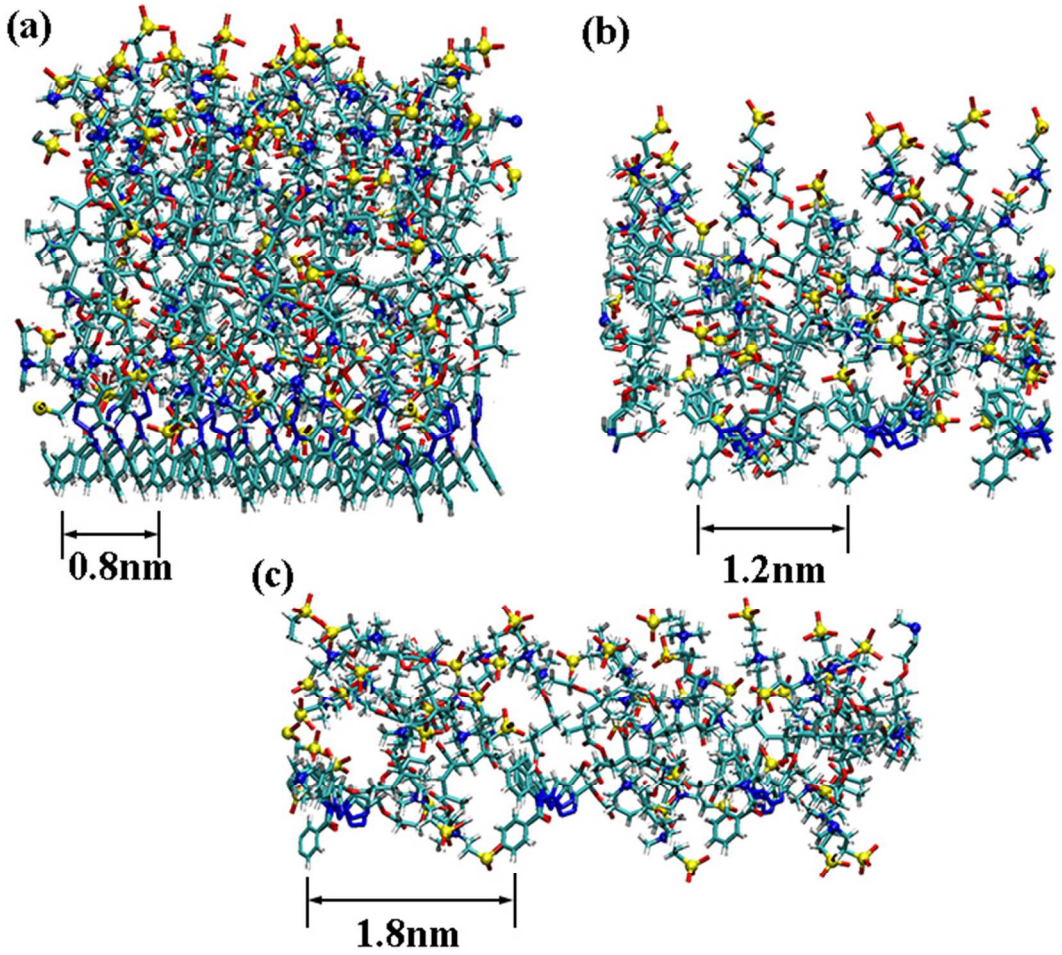

Figure 6. Snapshots of (a) high-grafting-density, (b) intermediate-grafting-density, and (c) low-grafting-density sulfobetaine brush arrays in hydrated states. Colors: red, O; white, H; light blue, C; dark blue, N; and yellow, S. The S atoms in sulfonate are in yellow and the N atoms in quaternary ammonium are in dark blue using ball presentation. Water molecules in these figures are not shown for clarity.

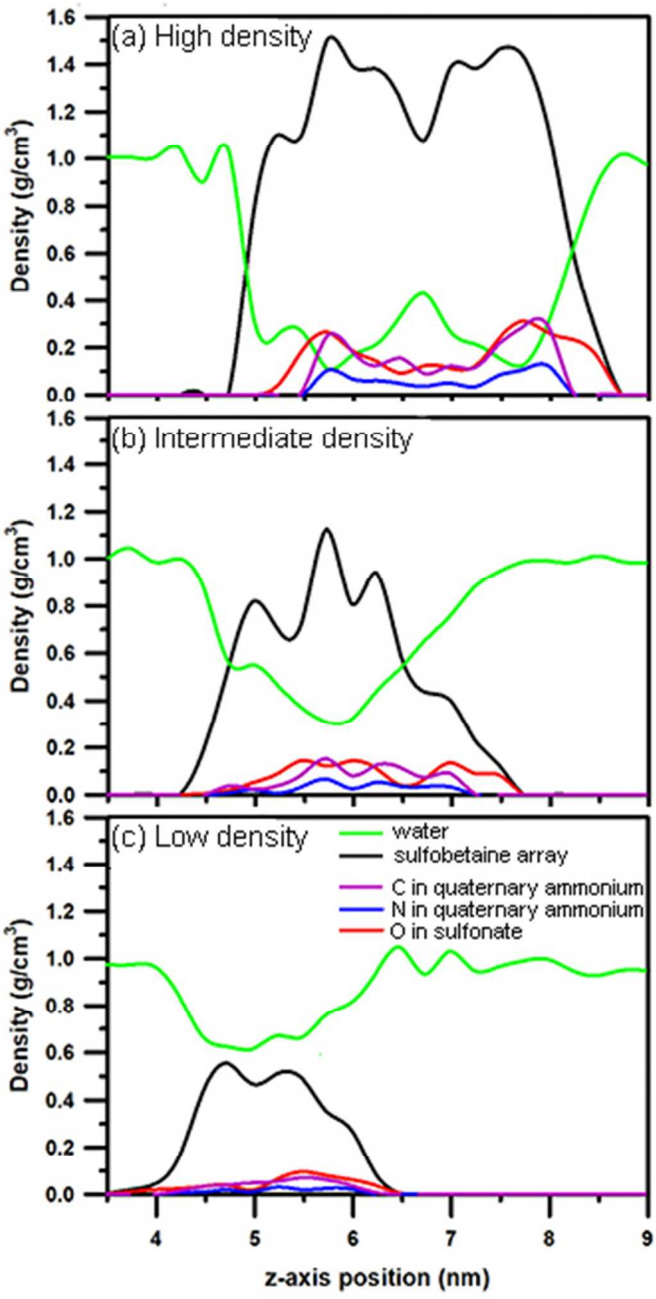

Figure 7. Material density profiles of the sulfobetaine brush arrays in hydrated states. Water density distribution is also shown in the figure. Panels (a), (b), and (c) correspond to the high-, intermediate-, and low-grafting-density brush arrays, respectively.

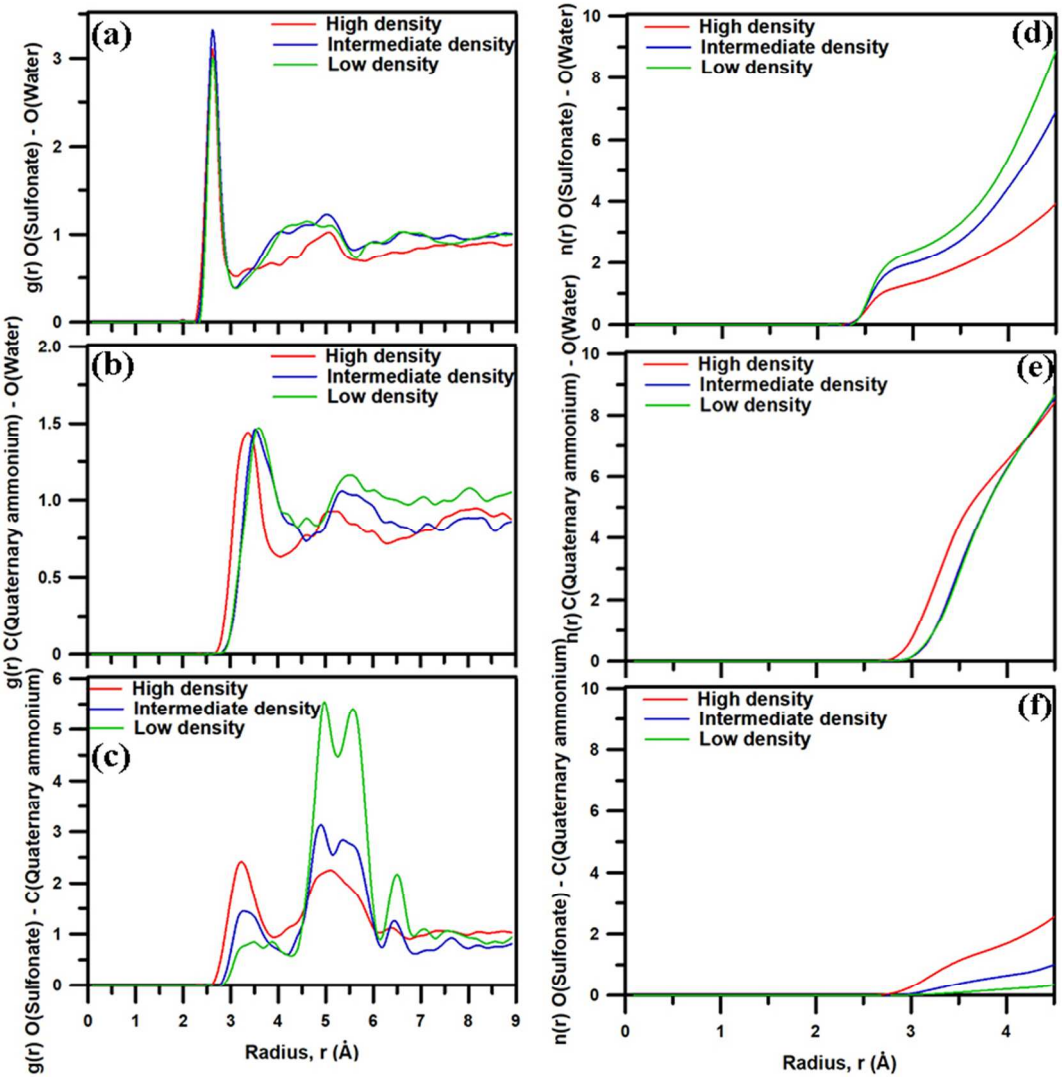

Figure 8. Radial distribution functions for the contact pairs between (a) oxygen atoms in sulfonate and water oxygen atoms; (b) carbon atoms in quaternary ammonium and water oxygen atoms; and (c) oxygen atoms in sulfonate and carbon atoms in quaternary ammonium. Panels (d), (e), and (f) correspond to coordination numbers of the three contact pairs, respectively.

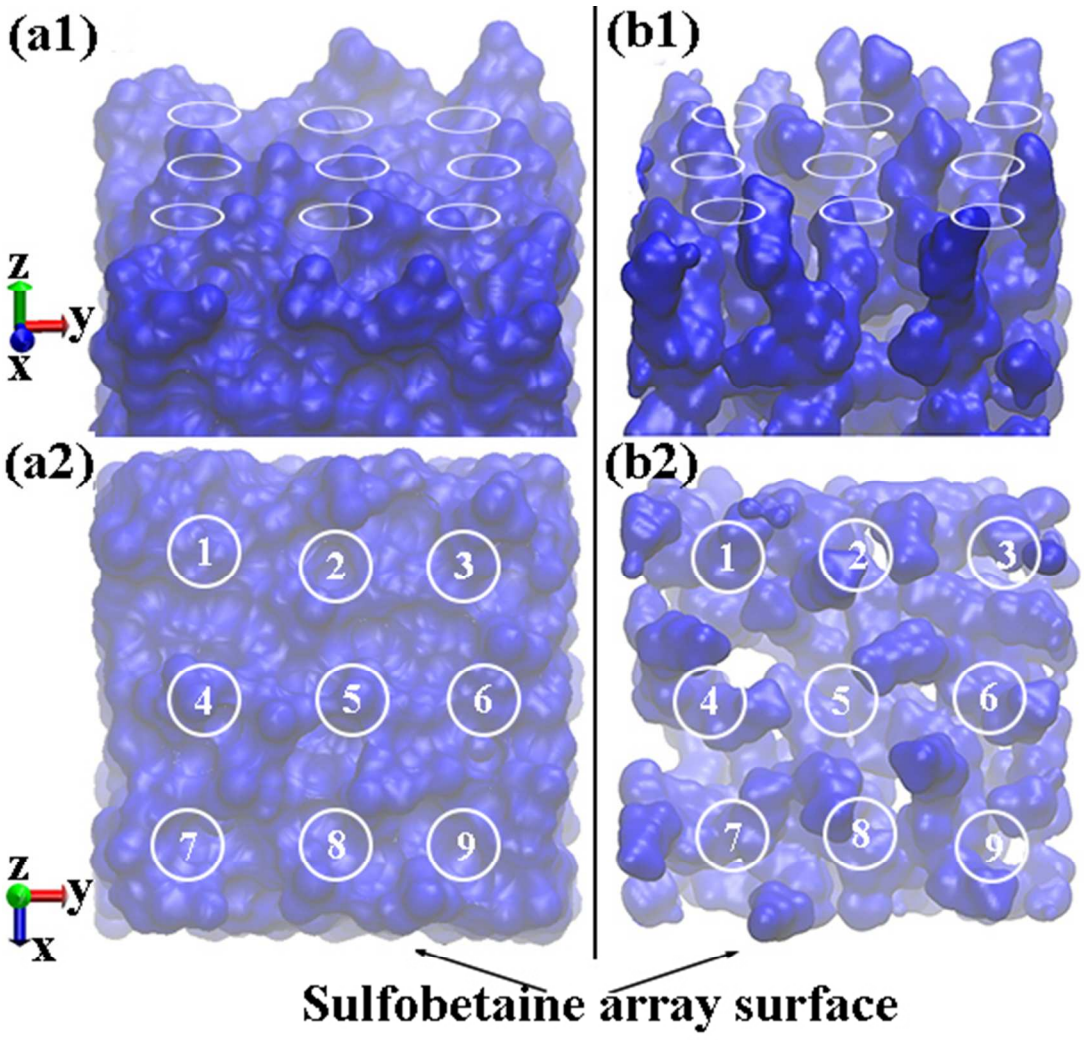

Figure 9. Snapshots of the sulfobetaine brush array surfaces with (a) high grafting density and (b) intermediate grafting density in equilibrium states. The sulfobetaine array surfaces are represented by the blue van der Waals contours. The white circles with different numbers indicate the locations at which independent steered molecular dynamics simulations are performed.

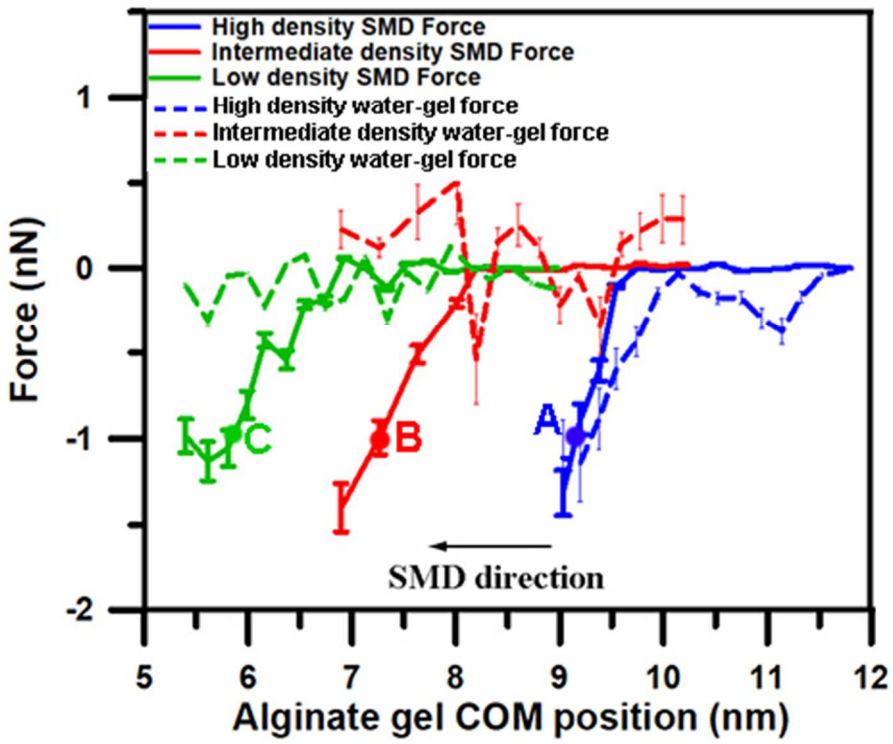

Figure 10. The force-distance profiles obtained from SMD simulations for the high-, intermediate-, and low-grafting-density array surfaces. The horizontal axis represents the position of COM of the alginate gel. Negative values correspond to repulsive spring forces.

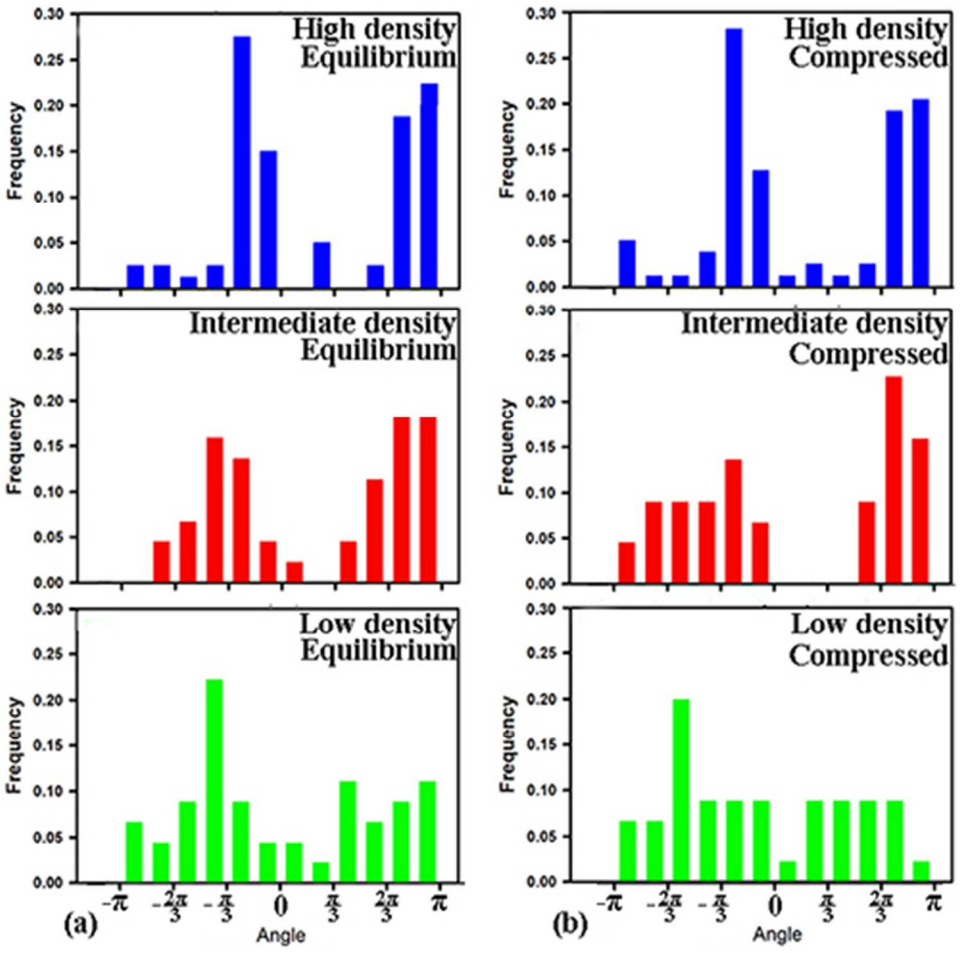

Figure 11. Histograms of branch orientations θ_{xy} for sulfobetaine brush arrays (a) in equilibrium states and (b) under compression of 1nN by an alginate gel. Angle θ_{xy} is defined in Figure 1c, which varies from –π to + π.

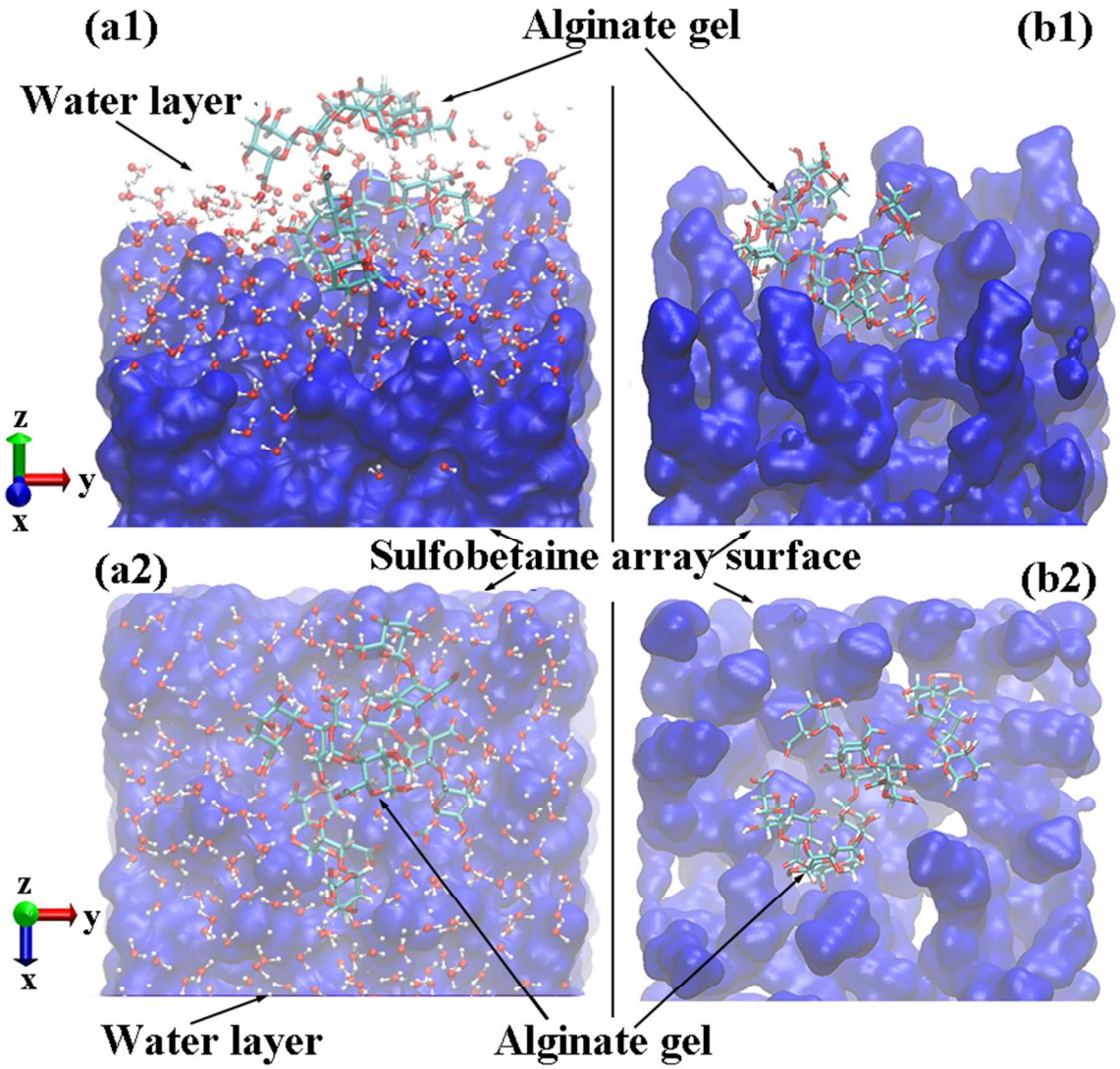

Figure 12. Snapshots of the sulfobetaine array surfaces with (a) high grafting density and (b) intermediate grafting density under compression of 1nN by an alginate gel. The sulfobetaine array surfaces are represented by the blue van der Waals contours. Hydration water layer near the high-grafting-density array surface is also shown. Hydration water layer near the intermediate-grafting-density array surface is not shown for clarity.

TOC Figure

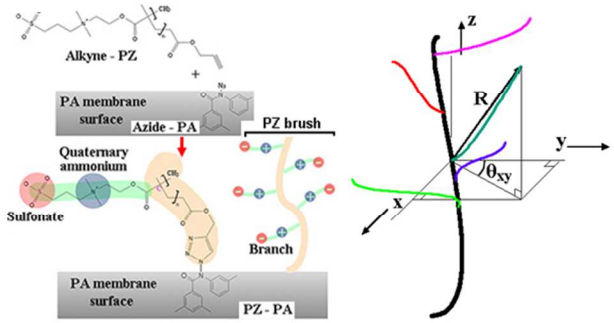
Alkyne - PZ
PA membrane surface
Azide - PA
PZ brush
Quaternary ammonium
Sulfonate
Branch
PA membrane surface
PZ - PA
z
R
y
x
θxy